The Astrophysical Journal Letters, 923:L26 (5pp), 2021 December 20 https://doi.org/10.3847/2041-8213/ac4014

Supernova Preshock Neutronization Burst as a Probe of Nonstandard Neutrino Interactions

Xu-Run Huang[1], Shuai Zha[2], and Lie-Wen Chen[1,†]
[1] School of Physics and Astronomy, Shanghai Key Laboratory for Particle Physics and Cosmology, and Key Laboratory for Particle Astrophysics and Cosmology (MOE), Shanghai Jiao Tong University, Shanghai 200240, People's Republic of China; lwchen@sjtu.edu.cn
[2] Tsung-Dao Lee Institute, Shanghai Jiao Tong University, Shanghai 200240, People's Republic of China
Received 2021 October 29; revised 2021 November 30; accepted 2021 December 4; published 2021 December 16

Abstract

A core-collapse supernova (CCSN) provides a unique astrophysical site for studying neutrino–matter interactions. Prior to the shock-breakout neutrino burst during the collapse of the iron core, a preshock ν_e burst arises from the electron capture of nuclei and it is sensitive to the low-energy coherent elastic neutrino–nucleus scattering (CEνNS) which dominates the neutrino opacity. Since the CEνNS depends strongly on nonstandard neutrino interactions (NSIs), which are completely beyond the standard model and yet to be determined, the detection of the preshock burst thus provides a clean way to extract the NSI information. Within the spherically symmetric general-relativistic hydrodynamic simulation for the CCSN, we investigate the NSI effects on the preshock burst. We find that the NSI can maximally enhance the peak luminosity of the preshock burst almost by a factor of three, reaching a value comparable to that of the shock-breakout burst. Future detection of the preshock burst will have critical implications on astrophysics, neutrino physics, and physics beyond the standard model.

Unified Astronomy Thesaurus concepts: Supernova neutrinos (1666)

1. Introduction

Neutrinos interact feebly with ordinary matter (Wolfenstein 1999). Nonetheless, they play a critical role in a core-collapse supernova (CCSN), which marks the death of massive stars with mass $\gtrsim 8\,M_\odot$ and leaves behind a compact remnant (see Woosley et al. 2002; Janka 2012; Burrows & Vartanyan 2021, for reviews). In a CCSN, most ($\sim$99%) of the released gravitational potential energy ($\sim 10^{53}$ erg) of the progenitor star is ultimately liberated through neutrino emission within a $\sim$10 s burst. Neutrinos from CCSNe can thus carry invaluable information on both CCSN and neutrino physics (Koshiba 2003).

Meanwhile, the discovery of neutrino oscillations (Fukuda et al. 1998; Ahmad et al. 2002) indicates neutrinos are massive and lepton flavors are mixed, providing solid experimental evidence of physics beyond the standard model (SM). Current and upcoming neutrino experiments can measure subdominant neutrino oscillation effects that are expected to give information on the yet-unknown neutrino parameters and the nonstandard interactions (NSIs) between neutrinos and matter (Wolfenstein 1978; Ohlsson 2013; Farzan & Tórtola 2018; Bhupal Dev et al. 2019). Note that the NSI are completely originated from new physics beyond the SM and not an expected consequence of existing theories or neutrino oscillations. The NSI can modify the production, propagation, and detection of neutrinos and thus may crucially affect the interpretation of the relevant experimental data. While the oscillation experiments can put important constraints on the NSI parameters, nonoscillation data (e.g., from neutrino-scattering experiments) are needed to break the possible degeneracy of the neutrino parameters allowed by oscillation data alone (Coloma et al. 2017). Indeed, the deep inelastic neutrino-scattering experiments (e.g., CHARM, Dorenbosch et al. 1986; and NuTeV,Zeller et al. 2002) can help to break degeneracy but the constraints apply only if the NSI are generated by mediators not much lighter than the electroweak scale. For light mediators (Denton et al. 2018), the degeneracy can only be broken through combination with results on coherent elastic neutrino–nucleus scattering (CEνNS), which was predicted in the 1970s (Freedman 1974) but observed only recently by the COHERENT Collaboration (Akimov et al. 2017, 2021).

Indeed, a global fit to neutrino oscillation and CEνNS data indicates that the degeneracy of neutrino parameters is significantly disfavored for a wider range of NSI models (Esteban et al. 2018; Farzan & Tórtola 2018; Coloma et al. 2020). Although significant progress has been made on constraining the NSI parameters by analyzing data on neutrino oscillations, deep inelastic neutrino scattering, and CEνNS, some NSI parameters are still not well constrained. In particular, the vector-like quark-ν_e neutral current (NC) couplings, ε_{ee}^{uV} and ε_{ee}^{dV}, are the least experimentally constrained (Esteban et al. 2018; Farzan & Tórtola 2018; Coloma et al. 2020), preserving parameter space large enough to cause sizable modifications in the CEνNS cross sections. Compared to the case of charged-current (CC) NSI, it is a much more daunting task to constrain NC NSI due to the experimental and theoretical difficulties. Because of the frequent CEνNS in a CCSN, the CCSN can thus provide an ideal site for constraining the NC NSI parameters. Recently, Suliga & Tamborra (2021) estimate the NSI effects on neutrino–nucleon scattering in the postbounce SN core within the diffusion time criterion wherein the neutrinos cannot be trapped for too long. In this work, we show that the neutrino burst from the preshock neutronization in a CCSN can be used as a novel and clean probe of the NC NSI parameters ε_{ee}^{uV} and ε_{ee}^{dV}.

† Author to whom any correspondence should be addressed.

2. Preshock Neutronization Burst

Modern CCSN models (O'Connor et al. 2018) have commonly predicted the existence of the so-called neutronization neutrino burst with a peak luminosity $\sim 4\times10^{53}\,\mathrm{erg\,s^{-1}}$, which emerges during the first ~25 ms after the core bounce as a result of sudden breakout of a flood of neutrinos freshly produced in shock-heated matter (and some ν_e produced previously that have diffused to the neutrinosphere) when the bounce shock penetrates the neutrinosphere and reaches the neutrino-transparent regime at sufficiently low densities. This shock-breakout burst mainly comprises ν_e from electron captures on free protons in the shock-heated matter.

Prior to the shock-breakout burst, a smaller burst exists that is due to ν_e produced from the preshock neutronization of the collapsing core (Liebendörfer et al. 2003; Kachelrieß et al. 2005; Wallace et al. 2016; O'Connor et al. 2018). This preshock burst emerges as a result of the competition between the ν_e emission due to electron captures on nuclei during the early neutronization stage of core collapse and ν_e trapping due to the opacity enhancement as the density and temperature of the core increase. Although the preshock burst is weaker than the shock-breakout burst, it generally has weaker model dependence in the CCSN simulations since it only involves relatively simpler dynamics in the early stage of the CCSN. In particular, the preshock burst is expected to strongly depend on the CEνNS cross sections which essentially control the neutrino opacity in the preshock stage (Bruenn & Mezzacappa 1997), and thus to provide a clean probe of the NC NSI parameters ε_{ee}^{uV} and ε_{ee}^{dV}. It should be noted that the NC interactions change the neutrino opacity without directly changing the neutrino production rate which is mainly determined by the CC electron capture processes (Sullivan et al. 2016; Langanke et al. 2021).

3. NSI Effects on Neutrino–nucleus Scattering

Following the spirit of effective four-fermion couplings in low-energy weak interactions, the NC NSI Lagrangian can be typically formulated as (Ohlsson 2013; Farzan & Tórtola 2018; Bhupal Dev et al. 2019)

$$\mathcal{L}_{\rm NSI}=-2\sqrt{2}\,G_{\rm F}\varepsilon_{\alpha\beta}^{fX}(\bar{\nu}_\alpha\gamma^\mu P_L\nu_\beta)(\bar{f}\gamma_\mu P_X f), \tag{1}$$

where $G_{\rm F}$ is the Fermi constant; $\varepsilon_{\alpha\beta}^{fX}$ denotes the NSI parameters with $\varepsilon_{\alpha\beta}^{fX}\sim 1$ corresponding to an NSI strength comparable to that of SM weak interactions; $\alpha,\ \beta\in\{e,\ \mu,\ \tau\}$ represent neutrino flavors; $f\in\{e,\ u,\ d\}$ is the matter field; and P_X with $X=L(R)$ represents the left(right) chirality projection operator. The NSI parameters are flavor-diagonal for $\alpha=\beta$, while the lepton flavor is violated and the NSI becomes flavor-changing for $\alpha\neq\beta$. Here we mainly focus on the flavor-diagonal NC vectorial NSI couplings of ν_e to the light quarks, i.e.,

$$\varepsilon_{ee}^{fV}=\varepsilon_{ee}^{fL}+\varepsilon_{ee}^{fR}, f\in\{u,\ d\}, \tag{2}$$

since they have relatively larger parameter space with $\varepsilon_{ee}^{uV}(\varepsilon_{ee}^{dV})\in[0.0,\ 0.5]$ while the amplitude of other NSI parameters has been tightly constrained to be $\lesssim 0.1$ (Esteban et al. 2018; Farzan & Tórtola 2018; Coloma et al. 2020). Note the SNO results (Aharmim et al. 2008) agree well with the prediction of the standard solar model, suggesting small NSI axial interactions and thus $\varepsilon_{ee}^{fL}\approx\varepsilon_{ee}^{fR}$. With $\varepsilon^{u(d)}\equiv\varepsilon_{ee}^{u(d)V}$, the effective NSI couplings to nucleons can thus be obtained as

$$\varepsilon^p=2\varepsilon^u+\varepsilon^d,\quad \varepsilon^n=\varepsilon^u+2\varepsilon^d. \tag{3}$$

For neutrino–matter interactions, we use here the neutrino interaction library *NuLib* (O'Connor 2015). In order to investigate the effects of the NC NSI parameters ε^u and ε^d, we modify the cross sections of the following isoenergetic reactions, $\nu_e+\alpha\longleftrightarrow\nu_e+\alpha$, $\nu_e+p\longleftrightarrow\nu_e+p$, $\nu_e+n\longleftrightarrow\nu_e+n$, $\nu_e+{}^{A}_{Z}X\longleftrightarrow\nu_e+{}^{A}_{Z}X$, and the corresponding reactions induced by $\bar{\nu}_e$. For (anti-)neutrino–nucleus scattering, the cross section includes three corrections (Burrows et al. 2006): the ion–ion correlation function $\langle\mathcal{S}_{\rm ion}\rangle$, the form factor term $\mathcal{C}_{\rm FF}$ and the electron polarization correction $\mathcal{C}_{\rm LOS}$. The expressions of the three corrections remain unchanged since they are irrelevant to the NC NSI parameters ε^u and ε^d. For simplicity, we neglect the weak magnetism corrections for antineutrinos (Horowitz 2002) since here we mainly focus on the neutronization burst in the early stage of CCSN, which mainly involves ν_e. In such a case, the cross section modification is rather straightforward, namely, we only need to replace the NC vector couplings $g_V^p=1/2-2\sin^2\theta_W$ and $g_V^n=-1/2$ in the SM, respectively, by $g_V^{p'}$ and $g_V^{n'}$ as

$$g_V^{p'}=g_V^p+\varepsilon^p,\quad g_V^{n'}=g_V^n+\varepsilon^n. \tag{4}$$

Correspondingly, the cross section expression is modified by replacing the weak charge of nucleus $\mathcal{Q}_W=-2(Zg_V^p+Ng_V^n)$ by $\mathcal{Q}_W'$ as

$$\mathcal{Q}_W'=\mathcal{Q}_W+\mathcal{Q}_W^{\rm NSI},\quad \mathcal{Q}_W^{\rm NSI}\equiv-2(Z\varepsilon^p+N\varepsilon^n). \tag{5}$$

The ratio of the neutrino–nucleus cross sections with and without NSI can be expressed as $\sigma_{\rm SM+NSI}/\sigma_{\rm SM}=\mathcal{Q}_W'^2/\mathcal{Q}_W^2$ (Burrows et al. 2006) if we neglect the corrections from $\mathcal{C}_{\rm FF}$ and $\mathcal{C}_{\rm LOS}$. To examine the NSI effects on neutrino–nucleus scattering, we plot in Figure 1 the ratio $\sigma_{\rm SM+NSI}/\sigma_{\rm SM}$ as a function of ε^d ($\varepsilon^u=0$) or ε^u ($\varepsilon^d=0$) for several typical nuclei, i.e., α, ^{12}C, ^{56}Fe and ^{208}Pb, as well as protons (p) and neutrons (n). One sees that the neutrino–nucleus cross sections can be drastically suppressed and even vanish around a certain value of ε^d (ε^u) depending on the isospin of the nucleus. This is due to the fact that the effective weak charge $\mathcal{Q}_W'$ may vanish for a certain value of ε^d (ε^u) satisfying the relation $Y_p(g_V^p+2\varepsilon^u+\varepsilon^d)+(1-Y_p)(g_V^n+\varepsilon^u+2\varepsilon^d)=0$, where $Y_p=Z/A$ is the proton fraction of the nucleus. One can easily find $\mathcal{Q}_W'=0$ when $\varepsilon^u+\varepsilon^d=0.159$ for nuclei with $N=Z$ (e.g., α, ^{12}C), and for more neutron-rich nuclei (e.g., ^{56}Fe, ^{208}Pb) with smaller Y_p, $\mathcal{Q}_W'=0$ generally leads to larger ε^d (ε^u), as shown in Figure 1. On the other hand, the neutrino-p(n) cross section exhibits relatively weak sensitivity to ε^d or ε^u. These features will lead to a number of interesting consequences on the neutrino burst in CCSN.

4. NSI Effects on Neutrino Burst

SN core collapse and bounce are simulated using the spherically symmetric general-relativistic hydrodynamic code *GR1D* (O'Connor & Ott 2010; O'Connor 2015). As a default of the CCSN simulation, we adopt the $15\,M_\odot$ solar-metallicity progenitor star (s15s7b2) from Woosley & Weaver (1995), and the SFHo equation of state (EOS) from Steiner et al. (2013) is used to describe the physics of stellar matter. Figure 2 shows the time evolution of all-flavor neutrino number and energy

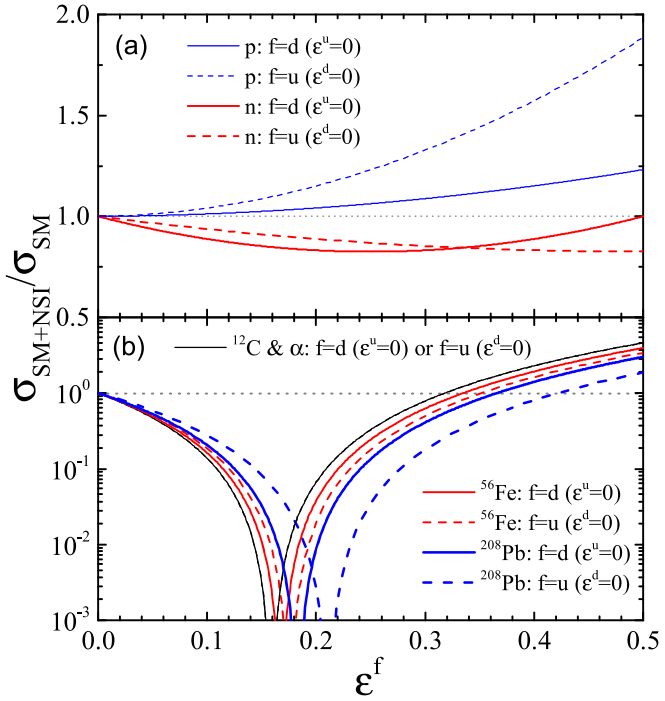

Figure 1. Neutrino–nucleon (a) and neutrino–nucleus (b) scattering cross sections divided by their SM model values as functions of the NSI parameter ε^d ($\varepsilon^u = 0$) or ε^u ($\varepsilon^d = 0$).

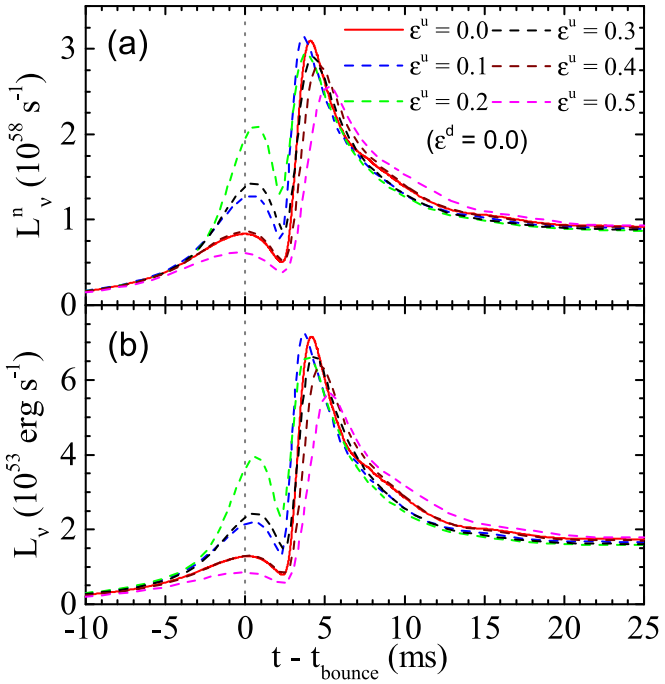

Figure 2. Time evolution of the total neutrino number (a) and energy (b) luminosities for the stellar collapse of a 15 $M_\odot$ solar-metallicity progenitor star using the SFHo EOS with various ε^u values ($\varepsilon^d = 0$).

luminosities in the initial two stages of CCSN, i.e., the infall phase and neutronization burst, with $\varepsilon^u = 0$, 0.1, 0.2, 0.3, 0.4, 0.5 ($\varepsilon^d = 0$). The later two stages of the accretion phase and Kelvin–Helmholtz cooling phase are not shown for simplicity since our main focus is the preshock burst.

For all the ε^u values considered here, it is clearly seen from Figure 2 that the luminosity displays two peaks, i.e., the smaller one around the bounce and the larger one after the bounce, respectively corresponding to the preshock burst and the shock-breakout burst. In particular, we note (although not shown here) that the preshock burst essentially consists of only ν_e, and the shock-breakout burst (around the peak) is also dominated by ν_e with $\lesssim$15% heavy-flavor (anti-)neutrinos and tiny ($\lesssim$1%) $\bar{\nu}_e$. In addition, the average ν_e energy of the preshock burst is $\sim$10 MeV. For the shock-breakout burst, the average energy is $\sim$14 MeV for ν_e, $\sim$15 MeV for heavy-flavor (anti-)neutrinos and $\sim$10 MeV for $\bar{\nu}_e$. These general features also have been observed in various modern CCSN simulations (O'Connor et al. 2018).

The most interesting feature illustrated in Figure 2 is the NSI effects on the two bursts, i.e., while the variation of the peak luminosity for the shock-breakout burst with ε^u is a little complicated and relatively weak ($\lesssim$10%), the corresponding variation for the preshock burst is rather straightforward and very drastic. For the latter, the peak luminosity first increases with ε^u varying from 0 to 0.2, and then decreases as ε^u changes from 0.2 to 0.5. Such a variation is mainly due to the NSI effects on the neutrino–nucleus scattering. As shown in Figure 1, increasing ε^u from 0 to $\sim$0.2 will reduce drastically the neutrino–nucleus cross section and even make it vanish at $\varepsilon^u \sim 0.2$, and the cross section enhances again as ε^u increases from $\sim$0.2 to 0.5. During the early neutronization stage of CCSN, the ν_e, e^-, and nuclei are dominant and the CEνNS decisively controls the neutrino opacity (Bruenn & Mezzacappa 1997). The suppression of neutrino–nucleus scattering will increase a neutrino's mean free path and thus enhance neutrino emission. Quantitatively, it is remarkable to see from Figure 2 that the peak number (energy) luminosity of the preshock burst can reach to $\sim 2.1 \times 10^{58}$ s^{-1} ($\sim 3.9 \times 10^{53}$ erg s^{-1}) for $\epsilon^u = 0.2$, which is significantly larger than and almost three times the corresponding value of without NSI (i.e., $\sim 0.86 \times 10^{58}$ s^{-1} ($\sim 1.3 \times 10^{53}$ erg s^{-1}) for $\epsilon^u = 0$), and it even becomes comparable to the corresponding result of the shock-breakout burst (i.e., $\sim 2.5 \times 10^{58}$ s^{-1} ($\sim 6.0 \times 10^{53}$ erg s^{-1})).

It is interesting to see that the peak luminosity of the shock-breakout burst does not much depend on the NSI, and this is understandable since the shock-breakout burst neutrinos are mainly produced through electron captures on free protons in the shock-heated matter and escape in the neutrino-transparent regime at sufficiently low densities where the neutrino–nucleus scattering is less important. The neutrino–nucleon scattering in the shock-heated matter may give rise to opacity and thus influence the neutrino emission of the shock-breakout burst, but the NSI effects are relatively weak as shown in Figure 1(a). Moreover, the preshock burst may also slightly influence the shock-breakout burst since the former affects the ν_e's distribution behind the neutrinosphere. Furthermore, modern CCSN simulations (O'Connor et al. 2018) indicate some sensitivity of the shock-breakout burst height and shape to the details of the neutrino transport, while the preshock burst is relatively robust due to the much simpler dynamics involved. Therefore, our results suggest that the preshock burst of CCSN should be a clean probe of the NSI.

To examine the robustness of the preshock burst as a probe of ε^f, we show in Figure 3 the peak number luminosity of the preshock burst as a function of ε^d ($\varepsilon^u = 0$) and ε^u ($\varepsilon^d = 0$) using three different EOSs, i.e., the default SFHo EOS, the LS220 EOS from Lattimer & Swesty (1991) with nuclear

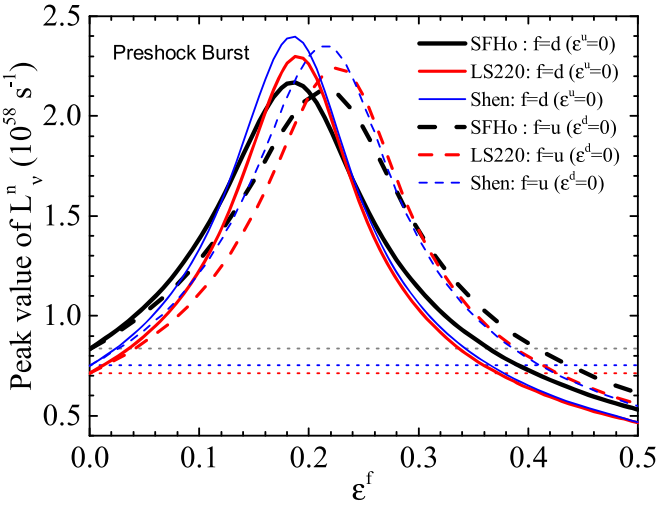

Figure 3. The total number luminosity peak value of the preshock burst vs. the NSI parameter ε^f for the stellar collapse of the $15\,M_\odot$ solar-metallicity progenitor star with three different EOSs, i.e., SFHo, LS220, and Shen. The dotted lines show the SM values for each EOS.

matter incompressibility $K_0 = 220$ MeV and Shen EOS from Shen et al. (2011). One sees that the difference of the peak number luminosity from the three EOSs is relatively small ($\sim$10%). The weak EOS dependence is mainly due to the small difference of low-density ($\lesssim 10^{12}$ g cm^{-3}) stellar matter EOS for the three EOSs since the preshock burst mainly involves stellar matter with density up to the neutrino-trapping value ($\sim 10^{12}$ g cm^{-3}). Indeed, using the Lattimer and Swesty EOSs (Lattimer & Swesty 1991) with $K_0 = 180$ MeV and 375 MeV which give very different EOS around and above nuclear density ($\gtrsim 10^{14}$ g cm^{-3}) but the same low-density EOS, we find the resulting peak number luminosities are almost the same as that with $K_0 = 220$ MeV. In addition, one sees from Figure 3 that the ε^f maximizing the peak number luminosity is larger than that minimizing the ν_e-^{56}Fe cross section as shown in Figure 1, and this is mainly because the ^{56}Fe nuclei in the collapsing core are transformed into more neutron-rich nuclei due to electron captures and thus larger ε^f is needed to minimize the ν_e-nucleus cross sections as discussed previously.

We also note the preshock burst only weakly depends on the progenitor mass, consistent with earlier findings (Takahashi et al. 2003; Kachelrieß et al. 2005; Wallace et al. 2016). Nevertheless, the progenitor property can be constrained with multimessenger signals (O'Connor & Ott 2013; Mukhopadhyay et al. 2020; Warren et al. 2020; Barker et al. 2021; Segerlund et al. 2021) once the source is detected. Moreover, the more realistic three-dimensional (3D) simulations (Nagakura et al. 2021) give very similar predictions on the neutronization burst during the early stage of CCSN as the one-dimensional (1D) simulations adopted here, further justifying the robustness of the preshock burst as a probe of ε^f. In addition, the nonstandard neutrino self-interactions (NSSI) are not considered here. Although the NSSI may significantly modify the neutrino-flavor transformation and thus influence the neutrino spectra (Dighe & Sen 2018; Yang & Kneller 2018; Lei et al. 2020), they are not expected to cause sizable modification to our results unless the NSI neutrino–neutrino coupling g_ν can be significantly larger than the NSI neutrino–quark coupling g_q (e.g., $g_\nu \gtrsim 90 g_q$). This is because the NSSI only have minor impact on the neutrino opacity due to the small ν_e fraction and cross section compared to those of nuclei in the early collapsing core. It will be interesting to see the NSSI effects on the preshock burst when the g_ν is extremely large (e.g., $g_\nu \gtrsim 90 g_q$).

In Figure 3, we consider only two extreme cases by independently varying ε^d ($\varepsilon^u = 0$) or ε^u ($\varepsilon^d = 0$), and the results with simultaneous variation of ε^d and ε^u should be between the corresponding results of the two extreme cases. Moreover, due to the quadratic dependence of the CEνNS cross section on the weak charge, there inevitably exists ε^f degeneracy for a fixed peak luminosity of the preshock burst. In particular, Figure 3 displays degeneracy for $\varepsilon^f = 0$ and $\varepsilon^f \sim 0.4$. The combined analysis of neutrino oscillation and CEνNS experiments perhaps can break the degeneracy. As pointed out in (Farzan & Tórtola 2018), $\varepsilon^d \simeq 0.3$ is more favored than $\varepsilon^d = 0$ at a level of 2 σ in analyses of solar neutrino experiments. Recently, the COHERENT collaboration report their new measurement of CEνNS on Argon, excluding the parameter region around $\varepsilon^f \sim 0.2$ with 90% C.L. (Akimov et al. 2021). Nevertheless, the peak luminosity of the preshock burst still keeps great sensitivity to the NSI in the remaining parameter space.

It is instructive to have a discussion on the experimental detection of the preshock burst. Although neutrino oscillation should not lead to major modifications to the core-collapse dynamics (Chakraborty et al. 2011; Dasgupta et al. 2012; Stapleford et al. 2020), it will largely distort the ν_e emission pattern in terrestrial detectors. Hence, it is better to use all-flavor detection to depict the temporal structure of the preshock burst. Recently, Raj (2020) shows the feasibility of detecting neutrino number luminosity from a failed CCSN using large-scale DM detectors, from which we note the detection of the preshock burst is possible if a source is located within $\sim$1 kpc. Luckily, such presupernova stars are not too rare in our galaxy, and a list of 31 candidates within 1 kpc, including the famous Betelgeuse, is rendered in Mukhopadhyay et al. (2020). In addition, the ε^f reduces the detection rate of the detectors made of nuclei but has no effects on the neutrino–electron cross sections and even enhances the neutrino-p cross sections, and therefore the detectors made of protons or electrons should be an ideal choice. As an example, we estimate the detection potential of ε^u by the Hyper-Kamiokande (Abe et al. 2018) via the electron-scattering channel. Using the *sntools* (Migenda et al. 2021) code to simulate the detector response for the preshock burst from a 1 kpc CCSN, we find the event count per 1 ms can reach $\mathcal{O}(10^2)$ around the preshock burst peak. By assuming $\chi^2 = \sum (N_{\rm SM} - N_{\rm NSI})^2/\sigma^2_{\rm stat.}$, we find the discovery region of ε^u with 3σ is [0.015, 0.388] $\oplus$ [0.415, 0.5] for no neutrino oscillation and [0.033(0.023), 0.373(0.380)] $\oplus$ [0.438 (0.424), 0.5] for the oscillation scenario with normal (inverted) neutrino-mass ordering. Furthermore, it is important to note that the flavor-blind measurement via the elastic neutrino-p scattering, e.g., in JUNO (An et al. 2016), can avoid the influence of oscillation and even break the degeneracy at $\varepsilon^f \sim 0.4$ due to the NSI enhancement of neutrino-p cross sections as shown in Figure 1(a). Such a detection configuration of JUNO is yet to be added in *sntools*.

Finally, we note that the enhancement of neutrino emission in the preshock burst can reduce the central electron fraction Y_e of the CCSN, e.g., the central Y_e after the bounce is reduced from 0.281 to 0.247 as ε^u varies from 0 to 0.2. This reduction of Y_e may influence the later neutrino flavor evolution,

explosion dynamics, and nucleosynthesis (Kajino et al. 2019; Cowan et al. 2021) of the CCSN. Reliable predictions on these topics are beyond the 1D simulations, and it will be extremely interesting to explore them within the more realistic 3D simulations (Nagakura et al. 2021). In addition, it is worth noting that the detection of the preshock burst may provide a clean way to extract neutrino oscillation information and determine the neutrino-mass hierarchies (Takahashi et al. 2003; Kachelrieß et al. 2005; Wallace et al. 2016).

5. Conclusion

We have demonstrated that the preshock neutrino burst in a CCSN can serve as a clean probe of the largely unknown NSI parameters ε_{ee}^{uV} and ε_{ee}^{dV}. In particular, our results indicate that the NSI can enhance the peak luminosity of the preshock burst almost by a factor of three and make the luminosity comparable to that of the shock-breakout burst, which will have critical implications on the explosion dynamics of CCSNs. Future detection of the preshock burst will open a new window to extract information on the CCSN, the NSI, the neutrino oscillation, and the neutrino-mass hierarchies.

The authors thank Jianglai Liu, Chuanle Sun, and Donglian Xu for useful discussions. This work was supported by the National SKA Program of China No. 2020SKA0120300 and the National Natural Science Foundation of China under grant No. 11625521.

Software: GR1D (O'Connor & Ott 2010; O'Connor 2015), NuLib (O'Connor 2015), sntools (Migenda et al. 2021).

ORCID iDs

Xu-Run Huang https://orcid.org/0000-0003-1842-8657
Shuai Zha https://orcid.org/0000-0001-6773-7830
Lie-Wen Chen https://orcid.org/0000-0002-7444-0629

References

Abe, K., Abe, K., Aihara, H., et al. 2018, arXiv:1805.04163
Aharmim, B., Ahmed, S. N., Amsbaugh, J. F., et al. 2008, PhRvL, 101, 111301
Ahmad, Q. R., Allen, R. C., Andersen, T. C., et al. 2002, PhRvL, 89, 011301
Akimov, D., Albert, J. B., An, P., et al. 2017, Sci, 357, 1123
Akimov, D., Albert, J. B., An, P., et al. 2021, PhRvL, 126, 012002
An, F., An, G., An, Q., et al. 2016, JPhG, 43, 030401
Barker, B. L., Harris, C. E., Warren, M. L., O'Connor, E. P., & Couch, S. M. 2021, arXiv:2102.01118
Bhupal Dev, P., Babu, K. S., Denton, P. B., et al. 2019, ScPPP, 2, 1
Bruenn, S. W., & Mezzacappa, A. 1997, PhRvD, 56, 7529
Burrows, A., Reddy, S., & Thompson, T. A. 2006, NuPhA, 777, 356
Burrows, A., & Vartanyan, D. 2021, Natur, 589, 29
Chakraborty, S., Fischer, T., Mirizzi, A., Saviano, N., & Tomàs, R. 2011, PhRvL, 107, 151101
Coloma, P., Denton, P. B., Gonzalez-Garcia, M. C., Maltoni, M., & Schwetz, T. 2017, JHEP, 2017, 116
Coloma, P., Esteban, I., Gonzalez-Garcia, M. C., & Maltoni, M. 2020, JHEP, 2020, 23
Cowan, J. J., Sneden, C., Lawler, J. E., et al. 2021, RvMP, 93, 015002
Dasgupta, B., O'Connor, E. P., & Ott, C. D. 2012, PhRvD, 85, 065008
Denton, P. B., Farzan, Y., & Shoemaker, I. M. 2018, JHEP, 07, 037
Dighe, A., & Sen, M. 2018, PhRvD, 97, 043011
Dorenbosch, J., Allaby, J. V., Amaldi, U., et al. 1986, PhLB, 180, 303
Esteban, I., Gonzalez-Garcia, M. C., Maltoni, M., Martinez-Soler, I., & Salvado, J. 2018, JHEP, 2018, 180
Farzan, Y., & Tórtola, M. 2018, FrP, 6, 10
Freedman, D. Z. 1974, PhRvD, 9, 1389
Fukuda, Y., Hayakawa, T., Ichihara, E., et al. 1998, PhRvL, 81, 1562
Horowitz, C. J. 2002, PhRvD, 65, 043001
Janka, H.-T. 2012, ARNPS, 62, 407
Kachelrieß, M., Tomàs, R., Buras, R., et al. 2005, PhRvD, 71, 063003
Kajino, T., Aoki, W., Balantekin, A. B., et al. 2019, PrPNP, 107, 109
Koshiba, M. 2003, RvMP, 75, 1011
Langanke, K., Martínez-Pinedo, G., & Zegers, R. G. T. 2021, RPPh, 84, 066301
Lattimer, J. M., & Swesty, F. D. 1991, NuPhA, 535, 331
Lei, M., Steinberg, N., & Wells, J. D. 2020, JHEP, 2020, 179
Liebendörfer, M., Mezzacappa, A., Messer, O. E. B., et al. 2003, NuPhA, 719, C144
Migenda, J., Cartwright, S., Kneale, L., et al. 2021, JOSS, 6, 2877
Mukhopadhyay, M., Lunardini, C., Timmes, F. X., & Zuber, K. 2020, ApJ, 899, 153
Nagakura, H., Burrows, A., Vartanyan, D., & Radice, D. 2021, MNRAS, 500, 696
O'Connor, E. 2015, ApJS, 219, 24
O'Connor, E., Bollig, R., Burrows, A., et al. 2018, JPhG, 45, 104001
O'Connor, E., & Ott, C. D. 2010, CQGra, 27, 114103
O'Connor, E., & Ott, C. D. 2013, ApJ, 762, 126
Ohlsson, T. 2013, RPPh, 76, 044201
Raj, N. 2020, PhRvL, 124, 141802
Segerlund, M., O'Sullivan, E., & O'Connor, E. 2021, arXiv:2101.10624
Shen, H., Toki, H., Oyamatsu, K., & Sumiyoshi, K. 2011, ApJS, 197, 20
Stapleford, C. J., Fröhlich, C., & Kneller, J. P. 2020, PhRvD, 102, 081301
Steiner, A. W., Hempel, M., & Fischer, T. 2013, ApJ, 774, 17
Suliga, A. M., & Tamborra, I. 2021, PhRvD, 103, 083002
Sullivan, C., O'Connor, E., Zegers, R. G. T., Grubb, T., & Austin, S. M. 2016, ApJ, 816, 44
Takahashi, K., Sato, K., Burrows, A., & Thompson, T. A. 2003, PhRvD, 68, 113009
Wallace, J., Burrows, A., & Dolence, J. C. 2016, ApJ, 817, 182
Warren, M. L., Couch, S. M., O'Connor, E. P., & Morozova, V. 2020, ApJ, 898, 139
Wolfenstein, L. 1978, PhRvD, 17, 2369
Wolfenstein, L. 1999, RvMP, 71, S140
Woosley, S., Heger, A., & Weaver, T. 2002, RvMP, 74, 1015
Woosley, S. E., & Weaver, T. A. 1995, ApJS, 101, 181
Yang, Y., & Kneller, J. P. 2018, PhRvD, 97, 103018
Zeller, G. P., McFarland, K. S., Adams, T., et al. 2002, PhRvL, 88, 091802